Nuclear Materials and Energy 33 (2022) 101306

Contents lists available at ScienceDirect

Nuclear Materials and Energy

journal homepage: www.elsevier.com/locate/nme

# 2D GEM-based SXR imaging diagnostics for plasma radiation: Preliminary design and simulations

Maryna Chernyshova [a,*], Karol Malinowski [a], Sławomir Jabłoński [a], Yevgen Melikhov [b], Andrzej Wojeński [c], Grzegorz Kasprowicz [c], Tomasz Fornal [a], Martin Imríšek [d], Fabien Jaulmes [d], Vladimir Weinzettl [d]

[a] Institute of Plasma Physics and Laser Microfusion, Hery 23, 01-497 Warsaw, Poland
[b] Institute of Fundamental Technological Research PAS, Pawinskiego 5B, 02-106 Warsaw, Poland
[c] Warsaw University of Technology, Institute of Electronic Systems, Nowowiejska 15/19, 00-665 Warsaw, Poland
[d] Institute of Plasma Physics CAS, Za Slovankou 1782/3, 18200 Prague, Czech Republic

ARTICLE INFO

*Keywords:*
Plasma physics
Plasma radiation diagnostics
SXR imaging detector
Micropattern gaseous detectors (MSGC, GEM, THGEM, RETHGEM, MHSP, MICROPIC, MICROMEGAS, InGrid, etc.)
Gas electron multiplier
Detector simulations

ABSTRACT

The purpose of this research is to design and construct a plasma radiation imaging system for fusion devices which is focused on soft X-ray region from about 2 to 15 keV photon energy. The proposed 2D diagnostic system, as opposed to conventional 1D systems, is expected to benefit from tangential field of view and to deliver new data for toroidal phenomena observations. This contribution relates to the introductory development of such 2D system laying out details on the overall design of the detecting unit (based on GEM technology) as well as on its acquisition module. The results cover also the expected photon flux and spectra foreseen for COMPASS-U device, as a first choice for testing and verification. Considerations on working medium and internal structure of the detecting sensor are presented including electrodes configurations and collecting electrode pattern. The preliminary establishments for data acquisition system are presented as well.

## 1. Introduction

Soft X-ray (SXR) detecting systems have been widely used in the plasma core of tokamaks and stellarators [1]. As SXR radiation could be originating from various processes involving electrons interacting with ions or external magnetic field, as bremsstrahlung, cyclotron emission, radiative recombination, de-excitation of atoms or ions, analysis of SXR radiation finds applicability in studying, among others, impurities and their profiles, in identification of core islands, MagnetoHydroDynamics (MHD) modes/localization, in plasmas impurities/MHD interplay, in studying first wall material erosion, for power exhaust programme [2] and its consecutive impact on plasma core. One of the examples of an application with high priority is development of SXR detecting system to identify presence, quantity and distribution of W in plasma for reactors in which W is chosen to be a first wall material. In view of construction of the first experimental reactor this is important due to the fact that even a small amount of highly radiative W in plasma could lead to a disruption [3]. Another key topic to be solved in order to secure a safe operation of ITER [4] corresponds to studying runaway electrons (RE) generation and disruption mitigation. Here, an imaging detector may also become a valuable tool for analysis of methods for RE effective mitigation, e.g., the ITER-proposed mitigation method - solid material pellet injection into the evolved runaway electron beam. This should create a spatially well localized source of bremsstrahlung radiation, spatially and energetically resolved measurements of which would be of use to evaluate the effectivity of mitigation system.

Among significant drawbacks of current tomography diagnostics based on SXR is their somewhat limited spatial resolution and/or cross-detector calibrations. Better spatial resolution is achieved for tangential imaging but advanced inversion techniques are required to interpret the obtained images due to the 3D line-of-sight integration [5]. It is believed however, that SXR 2D plasma photon counting imaging [6] has a huge potential in magnetic fusion experiments. Within this work, with the use of Gas Electron Multiplier (GEM) technology, it is aimed to develop 2D diagnostics that will be able to perform the global SXR imaging in photon counting mode (spectral response to be determined), to study the 3D phenomena of tokamak plasma, best measured by toroidal cameras, in the perspectives of ITER/DEMO. The uniqueness will involve 3D

* Corresponding author.
*E-mail address:* maryna.chernyshova@ipplm.pl (M. Chernyshova).

https://doi.org/10.1016/j.nme.2022.101306
Received 30 June 2022; Received in revised form 26 September 2022; Accepted 9 November 2022
Available online 14 November 2022
2352-1791/© 2022 Institute of Plasma Physics and Laser Microfusion, Warsaw, Poland. Published by Elsevier Ltd. This is an open access article under the CC BY-NC-ND license (http://creativecommons.org/licenses/by-nc-nd/4.0/).

plasma tomography, a feature greatly exceeding abilities of conventional tomography that will provide an opportunity to detect and study some toroidal anisotropy (that has been hardly explored so far) that originates from the non-axisymmetry of the plasma.

This contribution presents the results from the ongoing development of the detector structure suitable for effective 2D imaging under intensive SXR photon fluxes inherent in plasma fusion environment. The paper is structured as follows. Section 2 addresses expected experimental conditions and provides estimation of the expected spectra at the detector surface for COMPASS Upgrade tokamak. Section 3 presents the results of the simulations of the detector internal structure aimed at optimization of electron amplification stage by adjusting the internal electrodes configuration to be suitable for low/high gas amplification/diffusion. It includes also the details of special design of the proposed readout structure. Initial considerations and preliminary design of the DAQ system are collected in Section 4. Finally, Section 5 summarizes the paper with the conclusions.

## 2. Experiment conditions and expected income

Tests of the to-be-built diagnostics are chosen on COMPASS-U device [7,8], a middle size tokamak but still very flexible machine, designed and constructed as a high magnetic field (5 T) device with metallic plasma facing components. SXR system installation in its early operation phase would allow testing diagnostics robustness, neutron resilience (at rather moderate conditions), fundamental properties to study the 3D phenomena of plasma, and various properties of plasma with global imaging in photon counting mode. At the initial stage of COMPASS-U operation, a gradual increase of the magnetic field and plasma performance is planned with the auxiliary heating of at least 1–2 MW to be already available. A strong core plasma MHD activity driven by (mainly high-Z) impurities is highly probable for this phase of operation as well

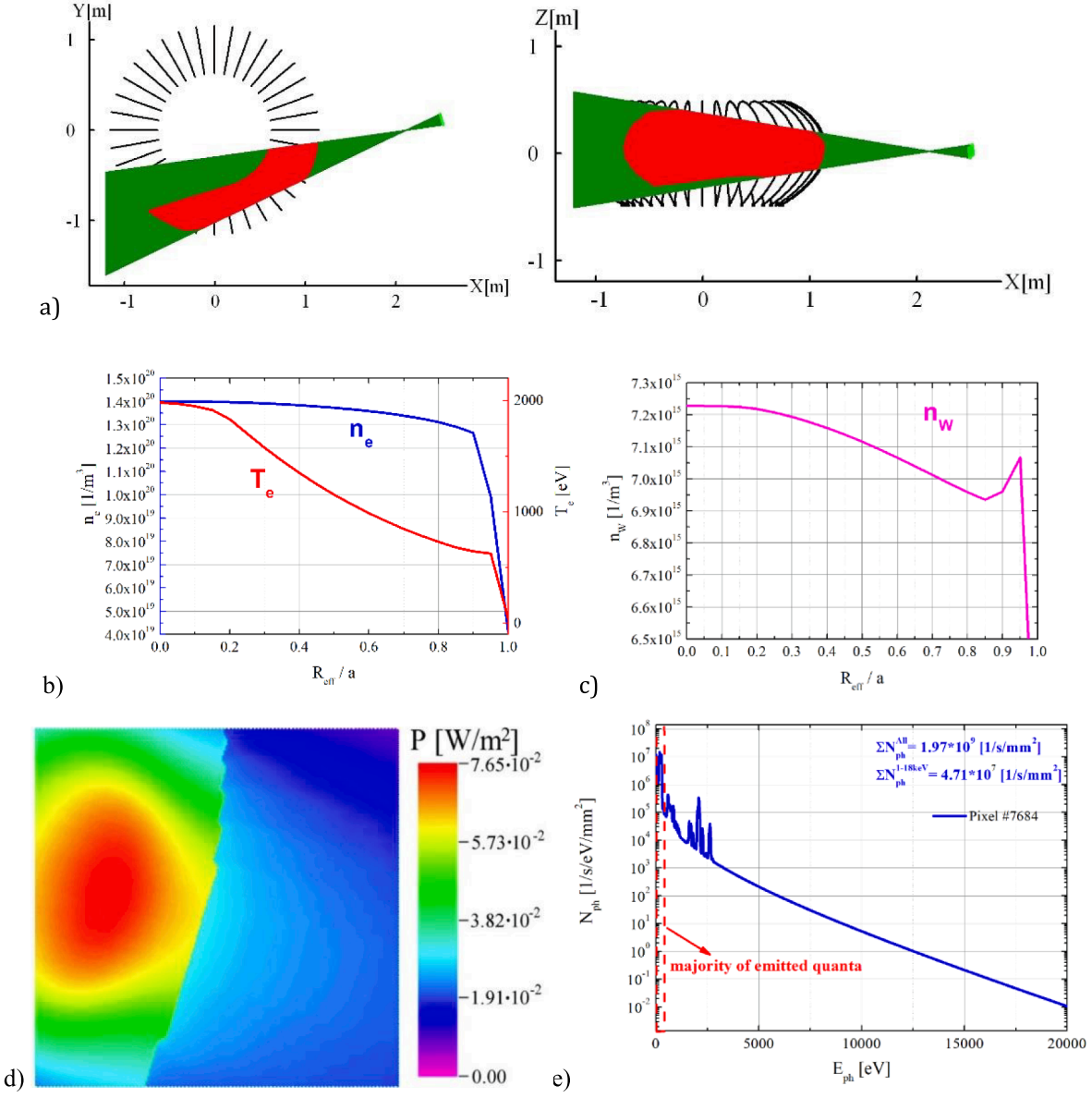


**Fig. 1.** (a) Outside port plug arrangement layout showing sensor and plasma contour, the red zone is the field of plasma volume view seen from the top and from the side. dimensions of the analyzed system elements are as follows: plasma height is 1000 mm, plasma width – 550 mm, major radius – 900 mm, distance pinhole-detector – 410.3 mm, pinhole diameter – 1 mm, side length of detector's hexagonal pixel – 0.350 mm; (b) electron density and temperature profiles considered for simulations, (c) tungsten concentration profile considered for simulations, (d) 2D power density distribution of calculated SXR emission; (e) spectrum for the most irradiated pixel. (For interpretation of the references to colour in this figure legend, the reader is referred to the web version of this article.)

as a significant fraction of RE in early plasmas. However, RE negative effects are considered to be still tolerable on smaller devices.

Wide X-shaped midplane diagnostic ports will allow installation of the detector in tangential as well as in radial directions, providing a different type of measured 2D data as an input for tomographic reconstructions. The preliminary geometry outline is presented in Fig. 1 (a). The outside port plug arrangement was chosen in order to simplify the diagnostics installation and integration to COMPASS-U at the same time giving possibility of some tangential view of the plasma.

In order to obtain rough information on the expected photon fluxes and spectra at COMPASS-U device a preliminary baseline plasma scenario #23400 for D-shaped plasma at lower parameters of plasma current (650 kA) and toroidal magnetic field (2.5 T) was considered for the first calculations. This scenario, foreseen for Phase 1, is a high-radiation physics relevant one at reasonable power output to plasma-facing components. The simulated electron density and temperature profiles, shown in Fig. 1(b)-(c) along with the tungsten profile, were taken during the developed H-mode at 1.245 s.

For the mentioned scenario calculations of the spectral and spatial distributions of X-ray photons in the range of 10 eV to 20 keV were conducted in order to estimate the expected radiation loads at the detector place. In terms of radiation emission from the plasma volume these simulations were made in the same way as reported in [9,10]. Three basic components of X-ray emission were considered for hydrogen plasma: continuous free-free (Bremsstrahlung), quasi-continuous free-bound (recombinant) and bound–bound (line emission) radiations. The entire preparation and simulation process has been divided into stages briefly described below.

Firstly, an etendue was calculated for the hexagonal pixel (see Section 3.4) located centrally under 1 mm diameter pinhole, $G_0$, using the expression for etendue of a long collimator. The etendue calculations were based on the numerical integration of the number of quanta emitted by a plasma volume of small/unit surface and 1 cm thickness, lying in the cone of view, to the pixel surface. In this way the etendue of the central pixel, $G_0$, was obtained. For the rest of detecting pixels the expression $G=G_0 \bullet \cos^4(\alpha)$ was used, where $\alpha$ is the angle between the normal to the pixel surface and the vector connecting the pinhole and pixel centers. It was found that within the whole detecting surface etendue deviation relative to the central pixel is within 6 %.

In the next step 2D distributions for the available 1D profiles of $T_e$, $n_e$ and $n_w$ were produced. For these data the cones of view with the central line of sight (LOS) for all the pixels were determined. Each cone was divided into a series of layers with a thickness of 1 cm perpendicular to the LOS. Within the layer, electron density and temperature, as well as tungsten concentration were assumed to be constant and determined by the central point of this layer. The discrepancy of the above-mentioned parameters within the layer was negligible (the results of analysis not shown here), which made such central point assumption a good estimate of the average value within the entire plasma layer.

The results of the calculations are shown in Fig. 1 (d)-(e). It can be seen that the power load of the detector for the considered arrangement is concentrated on one side of the detecting surface, whose LOSs are significantly longer than for the other part. As for spectral data, which were obtained using Open ADAS database for tungsten radiation simulation (ADF15 database for photon emissivity coefficients and ADF11 database for effective recombination and ionization coefficients), only low photon energy W lines (i.e., quasi-continuous radiation at about 2 keV) are foreseen for this scenario giving the moderate electron temperature. The analysis of the obtained X-ray spectrum for the most irradiated pixel shows that the majority of emitted quanta (over 90 %) comes from the photons of energy less than 300 eV (see Fig. 1). Thus, if needed, it would be easy to reduce the total number of photons up to an acceptable level.

It should be noticed that for further analysis more impurities than just W should be accounted for, e.g., Ni, considering the Inconel-based first wall materials. As for the contribution of individual tungsten ions to the line radiation within the given range of electron temperature profile (from 0.625 to 2 keV), ions from $W^{22+}$ to $W^{38}W^{+}$ were found. Tungsten ions with ionization degrees from 22+ to 37+ compose the linear spectrum up to 1 keV, whilst radiation from $W^{38+}$ ion, despite the relatively low fractional abundance for this temperature range (reaching only 2.5 %), dominates in the range of 1.118 to 2.635 keV. The line at 2.078 keV is of extremely high intensity.

## 3. Detector design and structure

### 3.1. General description

The detector aimed at 2D imaging capabilities was assumed to be a 2D Triple-GEM detector [11,12], with typically used electrode distances of 5/2/2/2 mm between cathode and the 1st GEM foil/the 1st and the 2nd GEM foils/the 2nd and 3rd GEM foils/the 3rd GEM and readout board, respectively. This arrangement, which is considered to be moderately complex, has been successfully examined in previous studies and allows for effective photon position and energy detection [10,12]. The fact that GEM detector can be built in stack, i.e., amplification stage of the detector can be multiplied, allows improving its stability by sharing generated charge between subsequent structures and spreading it between several GEM holes.

The detector's position, shown schematically in Fig. 1 (a), was chosen with the following objectives in mind: to cover as much as possible of the tangential view of the plasma (access to anisotropy plasma phenomena) and to allow relatively simple system installation. Giving the relatively big detecting surface (~10×10 $cm^2$), it is also advantageous to keep the absorbed flux well below the saturation limits of GEM detectors (~$10^6$ counts/$mm^2$s of absorbed radiation at a gas gain of ~$10^3$ and ~8 keV of incident radiation energy [13]), to avoid strong variation of the detector's amplification with the incident intensity due to the space charge accumulation.

One of the crucial parts of the imaging systems is its imaging plate or readout structure which should enable satisfactory spatial resolution of the detected radiation. For the elaborated detecting system, a pixel readout is proposed which is motivated by achieving good spatial resolution (limited by the pad size as $pitch/\sqrt{12}$), smaller input noise (implying input capacitance limits, decided to be kept below 10 pF) and a reasonable number of individual electronics channels (~3,000 within this work).

Addition of the radiation energy discrimination to the capabilities of the system entails requirement for single-photon counting mode and depends upon quality of the gas chamber electromechanics (arrangement of sequent electrodes), applied high voltage values and charge diffusion (influenced, e.g., by gas properties), etc.

Within the present work the main parameters of the detecting system to be established are the ones to enable its operation at a very low gas amplification (~1000), leading to extremely small signals (<10 fC), keeping at the same time high efficiency of the photon detection. This makes the whole development highly challenging in view of the competing goals: on the one hand to suppress the gas ionization and to reduce the current density (achieving lower gain, less aging and smaller space charge effect), on the other hand to make sure that acquisition system is able to record the photon generated pulses (a need for high charge sensitivity).

### 3.2. Gas mixture choice

The imaging system under development should be able to sustain high fluxes of photons in order to obtain high quality image. That implies high currents in terms of gas chamber operation that in turn might increase significantly the probability of spontaneous discharges. Therefore, it is important to define the working gaseous medium not only under fulfilment of the goal of effective photon detection but also under mitigation of spontaneous discharges (which, e.g., for $CO_2$ is

related to saturation of transfer rate [14]), streamer formation, etc. Usually, a mixture of noble gas (argon, neon, helium or xenon) and quenching agent is used for micropattern gas detectors (MPGD). Within this work a typical 70/30 $Ar/CO_2$ mixture was selected proven its applicability in other GEM-related works.

The calculated quantum detecting efficiency (QDE) shows that $Ar/CO_2$ mixture presents satisfactory photon detection efficiency in an SXR energy range [15]. Besides QDE, there are other gas parameters, e.g., electron drift/diffusion properties, which should be accounted for in order to achieve good readout signals of suitable spatial distribution. From this perspective Ar-composed mixture might be more beneficial given slightly larger electron radial diffusion expressed as a ratio to mobility than, e.g., in Ne (7.70 vs ~5 V [16] at the reduced electric field related to ab. 3 kV/cm and atmospheric pressure/room temperature for Ar and Ne, respectively) and lower electron drift velocity ($9.56 \bullet 10^3$ vs $35 \bullet 10^3$ m/s [16]) leading to more spatially spread electron avalanches. In order to have as large as possible spread of the electron cloud (to be discussed in Sections 3.3–3.4), higher electron energy (sum of the energy resulting from thermal motion and one obtained from the field), below the Townsend's ionization limit, is favorable with low/moderate drift field strength, resulting in low drift velocity. On the other hand, recalling that reduced $Ar^+$ ions mobility in Ar is approximately-three times lower than that of $Ne^+$ ions in Ne (1.52 vs 4.08 $cm^2V^{-1}s^{-1}$), the space charge effect might become significant at certain rates, as the ion backflow is similar for these two noble gases [17]. In addition, a little Kr admixture might be investigated in view of QDE enhancement at high photon energies as well as Ne-based gas medium. These considerations confirm the fact that optimization of the gas mixture is a complex task in itself, which will be performed later and reported elsewhere.

### 3.3. Amplification stage structure

The electrons and ions created by ionizing radiation in the conversion gap drift towards the corresponding electrodes. Electrons, amplified within GEM foil holes, move towards the subsequent GEM foil, finally, inducing a signal on the readout pattern. The aim of a multiplication stage of the detector is to achieve a measurable by an individual electronics channel signal at the level of ab. 3–10 fC and electron avalanche distribution on a minimal number of pixels necessary for unambiguous avalanche position identification. Thus, gas amplification was considered to be of order $\sim 10^3$ ensuring stable operation at high rates (below the upper limit $\sim 10^6$ c/$mm^2$s) without space charge accumulation. The considered high voltage (HV) values to be applied to each electrode were selected to maintain the targeted gain as well as to achieve acceptable spatial distribution of the electron cloud.

In order to achieve spatial diffusion of the generated charge matching to the readout structure and sufficient for good spatial resolution (up to the GEM detector limits at the level of 100 μm) and photon location identification on the detecting surface, different configurations of the GEM foils were examined. Here, the preliminary goal was to expand the electron spot resulting from photons with energies in the range from 2 keV to 15 keV onto at least 2 pixels of the patterned signal readout structure, similar to the one proposed in [18]. Within these preliminary studies, for estimation of electron transmission, 5.9 keV incident photons, which correspond to emission of $^{55}Fe$ radiation source usually used in the laboratory experiments, were considered. The pixel was assumed to be a hexagon with 0.35 mm side. The adopted HV values were adjusted in order to obtain the mentioned low gas gain as well as to keep certain conversion and transfer electric field, 3 kV/cm, in order to adjust the electron energy, obtained from the electric field, to the one for maximum of elastic scattering cross-section of Ar at ab. 10 eV [16].

Simulations of the spatial distribution of primary electrons were performed in Degrad [19] and of secondary electrons in Garfield++ [20]. Despite giving inadequate absolute numbers for the avalanche multiplication factor, Garfield++ produces a realistic estimate of its shape (since the avalanche shape depends weakly on the Monte-Carlo step size) predicting the relative spatial charge distribution with satisfactory precision [21]. Therefore, just *relative* comparison between the configurations will be performed. The absolute value of the avalanche should be finally defined experimentally.

For the sake of computing time and clear/straight comparison between various calculations the same randomly selected sets out of (maximally) 1,000 different spatial distributions of the primary electrons were used for the simulations of Triple-GEM detector (an example of such distribution is shown in Fig. 2). The input parameters for the avalanche were the coordinates of successive thermal electrons within the distribution with the randomly assumed avalanche center of gravity within the conversion/drift region.

In order to operate at the minimized charging up effect [13] cylindrical holes of 50 μm diameter were selected as a first choice. It should be noticed that the electron collection/transfer efficiency of GEM foil for the chosen electric fields might not be optimal for this hole shape, nevertheless, its usage is still qualified for straightforward comparison between different pitches. Under an assumption that different hole pitch could vary the transverse diffusion of the electron cloud moving to the readout anode, a range of hole spacing from 100 up to 300 μm was examined. The obtained, from performed $10^5$ Degrad calculations, average size of the primary electrons spot in conversion region was characterized by FWHM of ~100 μm (at 2.4 kV/cm field). Thus, the 300 μm pitch is considered as an upper limit for the simulations and adopted input parameters. Numerous preliminary simulations for configurations of different pitches and applied HV were performed. Also, adding double conical holes in the GEM foil with a large pitch (to improve the electron collection efficiency of the first foil) was examined.

At first, *Single*-GEM configurations were simulated and electron avalanche FWHM for different pitches within the range of 100 to 300 μm were identified. The results of the averaged electron avalanche, calculated using raw data interpolation (Fig. 3), present a saturation of the electron cloud spread for 100–180 μm spacing.

As a next step, *Triple*-GEM detector was modelled with different combinations of the GEM foil pitches. The standard configurations for all of the GEM foils from 100 to 300 μm were used. Along with the *regular* arrangement of the pitch values (e.g., 140/140/140 μm commonly used for GEM1/GEM2/GEM3 foils) *mixed* combinations were exploited, e.g., using decreasing pitch towards the readout anode for each subsequent GEM foil. Such an arrangement might be more favorable as an enlarging electron cloud will be shared within increased number of GEM holes. The obtained preliminary results show that the *average* FWHM of electron avalanche size is similar, 580–590 μm, for any choice of (regular) pitches for the Triple-GEM.

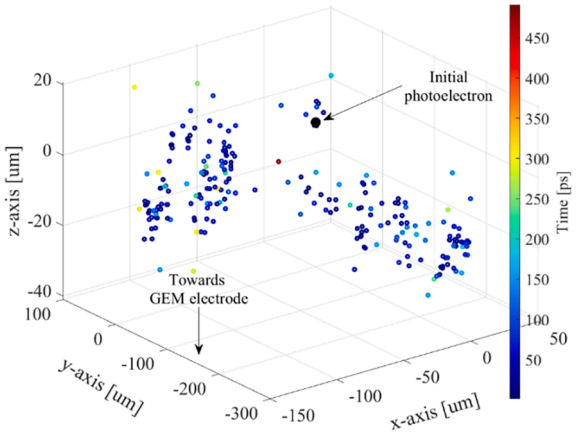


**Fig. 2.** Spatial distribution of thermal (primary) electrons created after absorption of 5.9 keV photon, including excitations, thermalized up to 2.0 eV energy in $Ar/CO_2$ gas mixture at 2.4 kV/cm conversion field. The initial photoelectron (in the center) is marked by a full circle.

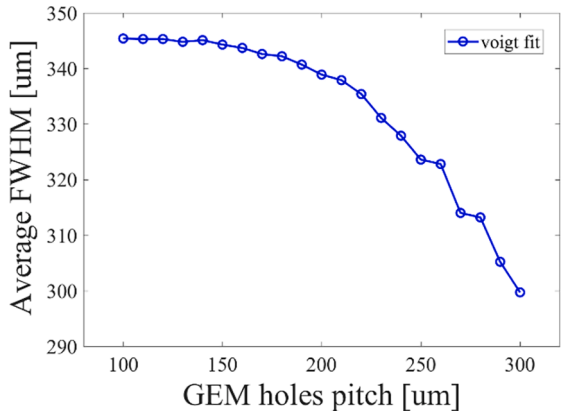


**Fig. 3.** Average FWHM (from Voigt fitting of single photon electron cloud shape) dependence on the GEM hole pitch for Single-GEM foil detector.

There are two factors that contribute to this result: geometrical/physical distances between holes (i.e., pitch) and extraction efficiency (that is related to electric field distribution that directs electrons towards those holes). In the case of the lesser pitch size, as in the case of Single-GEM simulations, the better electron extraction exists for the chosen electric field. This results in a larger avalanche size for smaller pitches, as is in the case of Single-GEM. Whereas for Triple-GEM the extraction efficiency is not optimal for the chosen electric field. On the other hand, from geometrical point of view, larger pitch in a Triple-GEM configuration tends to spread the avalanche onto a larger surface. That is why the resulting avalanche size is more unified within the whole pitch range for Triple-GEM than it might have been expected considering the Single-GEM results. In that sense, it reveals a tendency for larger pitches to result in more spread electron cloud for multiple foil configuration.

A comparison of results for selected regular and mixed configurations is presented in Fig. 4. For regular configurations with the large pitch a tendency of the distribution widening is observed as compared to the standard GEM based configuration (140/140/140 μm). It should be mentioned that the pitch values of different GEM foils should rather conserve a multiplicity to avoid possible parallel alignment of the foils with respect to each other.

Besides rather small obtained differences in the avalanche spread (all distributions of FWHMs are mostly in the range of ab. 500–750 μm), it might be crucial to have avalanche cutting across the single pixel boundary, therefore achieving photon position identification and keeping the reasonable number of DAQ channels. As can be seen in Fig. 4

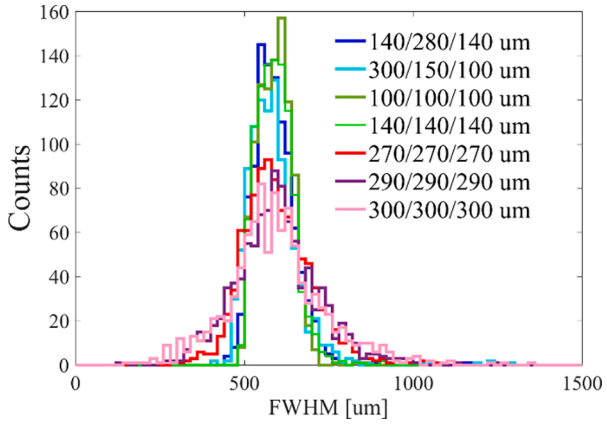


**Fig. 4.** Histograms of the obtained FWHM values for all the single photon avalanches for each configuration at 1500/600/600/600 V applied at D/T1/T2/I gaps between window, GEM foils and anode. HV applied at GEM foils was either 370 V for 300/150/100 μm configuration or 365 V for the rest of the simulations.

for large pitches (e.g., 290 μm), the electron avalanche extends onto larger areas but at the same time the FWHM distribution worsens and gets wider. The reason of this worsening lays in reduction of the amplification capabilities of multiple foil configuration. In Fig. 5 the average effective gain for all regular Triple-GEM configurations is shown. As can be noticed the multiplication capabilities are worsened towards the larger hole pitches. As was already mentioned it is most likely related to non-optimal collection/extraction efficiencies for the considered configurations. Apart from the pitch spacing impact itself, the electron transport in the detector chamber is driven by the electric field distribution defined by HV on all the electrodes (through GEM foils and all the gaps – drift (D), transfers (T1 and T2) and induction gaps (I)). Determining optimal HV values requires numerous simulations and/or measurements as were, for example, performed in [13]. There, it was observed that almost any attempt to increase the effective electron gain by varying voltages on GEM or different gaps, besides other effects, worsened the avalanche transverse diffusion. Therefore, if higher amplification is necessary, an addition of the 4$^{th}$ GEM foil with an additional multiplication factor of ab. 10 could be considered such as, e.g., the one with 100 μm pitch for effective electron collection and transmission to the anode. The associated elongation of the electron avalanche transfer time should not affect noticeably the exposure time resolution. Considering also the fact that for a multiple foil structure the optimum electron transparency may not result in optimum for other characteristics, as e.g. energy resolution, configurations with smaller pitches like, e.g., 100–120 μm, might be more preferential as a first choice. Nevertheless, further high statistics numerical studies are planned for large pitches as well.

The averaged avalanche distribution on the readout patterned structure for Triple-GEM is shown in Fig. 6 for the centered, with respect to each other, averaged electron avalanche and hexagon pixel, i.e., the most difficult case in terms of photon position identification as it challenges the DAQ system charge sensitivity. As it can be seen for the selected configuration the charge share within the neighboring pixels might be sufficient for measurements by the dedicated DAQ system. In case of the need to increase the generated charge (e.g., lower energy photons, unfavorable signal-to-noise ratio) further improvements can be performed.

Summarizing the obtained first results, further electric field optimization and high statistics (though highly time-consuming) simulations are needed as other geometry parameters, such as hole size/shape, insulator thickness, etc., may have an impact on the avalanche diffusion.

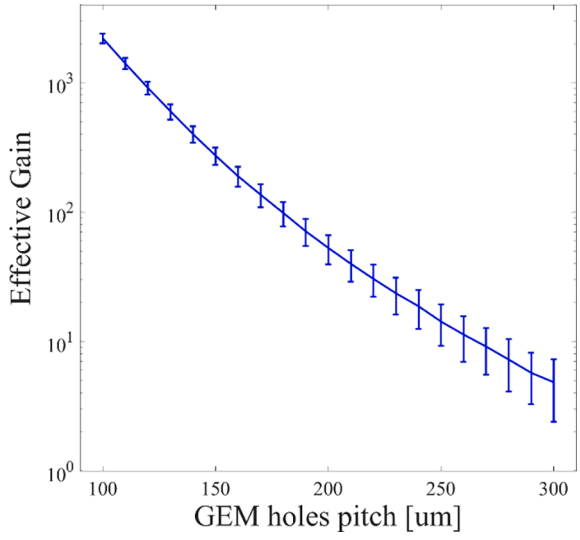


**Fig. 5.** Average effective gain calculated for the signals obtained for different pitch Triple-GEM configurations along with its standard deviation (bars).

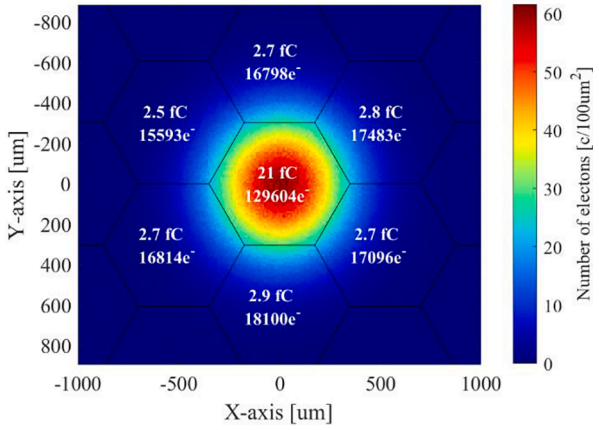


**Fig. 6.** 2D map of the averaged electron density along with the readout pixels for all the avalanches generated for the configuration of 100/180/100 μm pitches for cylindrical/double-conical/cylindrical GEM holes and ~700 effective gain.

### *3.4. 2D readout structure*

GEM detectors are characterized by separation of the processes of charge transfer/amplification from charge collection (i.e., signal reading) zone. That allows developing sophisticated readout structures with the possibilities to accustom them for specific experimental needs. With the aim to collect (i.e., to determine energy and position) of as many and as fast absorbed photons (and, therefore, electron clouds) as possible within the detector limits, one would require as many independent pixels as possible to be on the readout plane. However, current electronics cannot cope with huge number of independent pixels/channels. Hence, a special arrangement should be employed, for which pixels are interconnected in a special way to form multipixels. One of the effective ways is explained in [18] in details and, using current layout and spatial dimensions of the detector, as well as knowing average size of electron cloud, it is estimated that 34,680 pixels are required (170×204 hexagons with 0.35 mm side cover ~102.75×106.75 $mm^2$) interconnected into 2,894 multipixels [18]. A slightly modified approach was applied in this work leading, altogether, to total of 33,462 pixels (169×198 hexagons with 0.35 mm side cover ~102×104 $mm^2$) interconnected into 3,010 multipixels (details of this approach will be published elsewhere). Despite the slightly larger number of multipixels (3,010 vs 2,894 obtained with approach from [18]) such optimization allowed elimination of all the repeating pairs of neighboring/adjacent pixels, therefore, allowing unambiguous identification of the avalanche position, even in a case it spreads onto two closest-neighbor pixels. At the same time, it allowed a decrease of the capacitance of each multipixel from ab. 16 pF to 10 pF maximally.

Within the scope of the development of plasma radiation imaging, this crucial imaging component of the detecting chamber will be further optimized to cover the targeted photon energy in the SXR region followed by the development of procedures and methods for photon position reconstruction and its energy estimation.

## 4. Acquisition module configuration

Electronics is another fundamental part of the detecting system and difficulties in its development arise due to strong demands on system design: simultaneous requirements of low noise, high gain, high linearity, and high time resolution. Moreover, another factor adding to the complexity of the system is a requirement to use radiation hardened microelectronics as high neutron flux could bring serious disturbances to the signal. In addition, optimization of power consumption as well cost-effectiveness should be taken into account.

Since reconstruction of the high rate 2D image requires a massively parallel approach using thousands of data acquisition channels, an untypical approach using a re-purposed Ultrasound AFE chipset (such as AFE5832 from Texas Instruments [22]) to acquire GEM detector signals has been employed. For this particular imaging system, the acquisition requires existence of 3,010 channels, each processing a few mega events per second, as opposed to the previously used design that could work only for a maximum of hundred channels and could not be that compact for such a large number of channels (front-end electronics especially) [23–25]. The processing chain consists of input channels based on transimpedance amplifiers connected directly to GEM pixel board. The chips are placed on a dedicated front-end module located very close to the GEM pixel board to minimize the capacitance which affects the input noise directly. The signal is then transferred to the MCM ADC placed on an FMC module and plugged into the carrier board equipped with FPGA. The raw signals coming from AFE stage are processed by the analogue frontend and digitalization stages by the selected Ultrasound AFE multichannel ICs. After FPGA computations, the data is transmitted over multi-gigabit transceivers to the server cluster for processing and storage (Fig. 7). To speed up the development and to decrease the costs, re-usage of as many off-the-shelf components as possible and development of only the necessary ones has been adopted. For this reason, the FMC standard was chosen due to the popularity of FPGA carrier boards in various standards.

After a final detector construction, consistent and accurate calibration of the system will be required. Before the start of the experimental studies, there is a plan to prepare and/or finalize, at a given stage, all the auxiliary systems and associated tasks (detector – radiation source vacuum interface, Helium buffer for low energy photons to pass, complex DAQ and processing electronics, necessary software and firmware, algorithms for data processing and calibration, etc.).

## 5. Summary

Successful detection of various properties of plasma, such as shape and spectra of plasma radiation and/or level of impurities, continues to be an important and desired task. Here, all aspects of the 2D imaging system based on GEM technology were investigated. The expected experimental conditions at COMPASS Upgrade tokamak were taken to estimate numerically the expected spectra at the detector surface. In order to provide such information, investigations on gas mixture, values of high voltage at electrodes, pitch and hole dimensions at GEM foils, 2D readout structure and acquisition module configuration have been started and are currently under intensive optimization process. More specifically, simulations to identify the optimal choice of (regular or mixed) pitches for the Triple-GEM configuration led to a result that the *average* full width at half maximum (FWHM) of electron avalanche size does not significantly depend on pitch. But, the spread of the avalanche becomes noticeably larger for configurations with the foils having larger pitches (desired effect). However, amplifications of such configurations suffer distinct decrease of the gain (not desired effect). Therefore, Triple-GEM configuration with a smaller (regular) pitch, e.g., 100–120 μm, will be validated for imaging purposes at this stage of the detector's development. In parallel, mixed pitch configurations will be examined further in order to find more favorable amplification capabilities of the detector. In case of the readout structure, a slightly modified approach to interconnect pixels into multipixels was proposed and will be utilized. Such optimization allowed elimination of all the repeating pairs of neighboring/adjacent pixels, therefore, allowing unambiguous identification of the avalanche position, even in a case it spreads onto two closest-neighbor pixels and, it also allowed a decrease of the capacitance of each multipixel from ab. 16 pF to 10 pF maximally. Finally, a new DAQ system was developed for this detecting system. Overall, the construction of the detecting system is on the way with preparation to conduct experiments at COMPASS Upgrade tokamak.

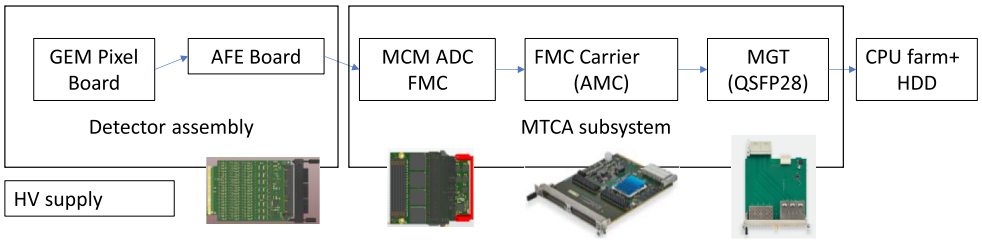


**Fig. 7.** Block diagram of DAQ system: 128-channel input section of the DAQ system consists of 128 transimpedance amplifiers (TIA) with protection; each card is connected to a dedicated FMC ADC board with four Texas AFE5832 MCM circuits; 24 FMC boards are on fast AMC carriers (AFCK boards); a companion board is used to provide a direct interface to route data to the server rack with processing and storage CPUs via standard QSFP fiber connectors. Small photos present render of 128-channel transimpedance amplifier card, 128-channel ADC FMC board, AFCK FMC carrier and RTM QSFP interface.

## CRediT authorship contribution statement

**Maryna Chernyshova:** Conceptualization, Methodology, Writing – original draft, Investigation, Writing – review & editing. **Karol Malinowski:** Software, Formal analysis, Validation, Software, Methodology. **Sławomir Jabłoński:** Software, Methodology, Investigation. **Yevgen Melikhov:** Writing – original draft, Investigation, Writing – review & editing. **Andrzej Wojeński:** Software, Validation, Writing – review & editing. **Grzegorz Kasprowicz:** Formal analysis, Investigation. **Tomasz Fornal:** Writing – review & editing, Visualization. **Martin Imríšek:** Software, Visualization. **Fabien Jaulmes:** Resources, Software, Visualization. **Vladimir Weinzettl:** Software, Writing – review & editing.

## Declaration of Competing Interest

The authors declare that they have no known competing financial interests or personal relationships that could have appeared to influence the work reported in this paper.

## Data availability

The authors are unable or have chosen not to specify which data has been used.

## Acknowledgements

This work has been carried out within the research project No. 2020/39/B/ST2/02681 financed by the National Science Center.

## References

[1] L. C. Ingesson et al., Chapter 7: tomography diagnostics: bolometry and soft-X-ray detection, Fusion Sci. Technol. 53 (2008) 528–576.
[2] R. Albanesea, et al., The DTT proposal. A tokamak facility to address exhaust challenges for DEMO: introduction and executive summary, Fus. Eng. Des. 122 (2017) 274–284.
[3] A. Kallenbach, et al., Tokamak operation with high-Z plasma facing components, Plasma Phys. Control. Fus. 47 (2005) B207.
[4] M. Lehnen, et al., Disruptions in ITER and strategies for their control and mitigation, J. Nucl. Mater. 463 (2015) 39–48.
[5] A. Wingen, et al., Regularization of soft-X-ray imaging in the DIII-D tokamak, J. Comput. Phys. 289 (2015) 83.
[6] D. Pacella, Energy-resolved X-ray detectors: the future of diagnostic imaging, Rep. Med. Imag. 8 (2015) 1–13.
[7] R. Panek, et al., Conceptual design of the COMPASS upgrade tokamak, Fusion Eng. Des. 123 (2017) 11–16.
[8] P. Vondracek, et al., Preliminary design of the COMPASS upgrade tokamak, Fusion Eng. Des. 169 (2021), 112490.
[9] S. Jablonski, et al., Simulation of pulse height analysis soft X-ray spectra expected from W7-X, J. Instrum. 10 (2015) P10021.
[10] M. Chernyshova, et al., First exploitation results of recently developed SXR GEM-based diagnostics at the WEST project, Nucl. Mater. Energy 25 (2020), 100850.
[11] F. Sauli, The gas electron multiplier (GEM): Operating principles and applications, Nucl. Instrum. Meth. Phys. Res. A 805 (2016) 2–24.
[12] M. Chernyshova, et al., 2D GEM based imaging detector readout capabilities from perspective of intense soft x-ray plasma radiation, Rev. Sci. Instrum. 89 (2018) 10G106.
[13] M. Chernyshova, et al., Study of the optimal configuration for a Gas Electron Multiplier aimed at plasma impurity radiation monitoring, Fusion Eng. Des. 136 (2018) 592–596.
[14] Ö. Şahin, et al., High-precision gas gain and energy transfer measurements in Ar-CO2 mixtures, Nucl. Instrum. Meth. Phys. Res. A 768 (2014) 104–111.
[15] M. Chernyshova, et al., Conceptual design and development of GEM based detecting system for tomographic tungsten focused transport monitoring, J. Instrum. 10 (2015) P10022.
[16] G.G. Raju, Gaseous Electronics: Tables, Atoms, and Molecules, CRC Press, 2018.
[17] The ALICE Collaboration. Upgrade of the ALICE Time Projection Chamber, CERN-LHCC-2013-020/ALICE-TDR-016, 2013. <http://cds.cern.ch/record/1622286>.
[18] M. Chernyshova, et al., Development of 2D GEM-based SXR plasma imaging for DTT device: focus on readout structure, Fusion Eng. Des. 169 (2021), 112443.
[19] S. Biagi, Transport of electrons in gas mixtures, 2019. <http://degrad.web.cern.ch/degrad/>.
[20] H. Schindler, R. Veenhof, Garfield++ simulation of ionisation based tracking detectors, 2018. <http://garfieldpp.web.cern.ch/garfieldpp/>.
[21] O. Bouianov, et al., Foil geometry effects on GEM characteristics, Nucl. Instrum. Meth. Phys. Res. A 458 (2001) 698.
[22] AFE5832: Product details, 2022. <https://www.ti.com/product/AFE5832>.
[23] A. Wojenski, et al., FPGA-based novel real-time evaluation and data quality monitoring system for tokamak high-performance GEM soft X-ray diagnostic, J. Instrum. 13 (2018) 2–18.
[24] G. Kasprowicz, et al., Multichannel data acquisition system for GEM detectors, J. Fusion Energy 38 (2019) 467–479.
[25] A. Wojenski, et al., Multichannel measurement system for extended SXR plasma diagnostics based on novel radiation-hard electronics, Fusion Eng. Des. 123 (2017) 727–731.